# CycloStride: Design and Development of a Prosthetic Knee Optimized for Level and Ramp Walking

Jared Grinberg[1], Nana Porter-Honicky[2], Paola Rioja[2], and C. Andrew Seelhoff[2]

***Abstract*— Transfemoral amputees exhibit substantial gait deviations during level and inclined walking because passive prosthetic knees cannot generate the positive and negative mechanical work required for normative stance-phase biomechanics. Fully powered knee–ankle systems can address this limitation but introduce mass, electrical, and control complexity that restrict daily usability. This work presents CycloStride, a powered-knee, passive-ankle prosthesis designed to provide functional assistance during both level-ground and ramp locomotion. The knee joint integrates a 1:8 cycloidal transmission driven by a 1:6 Dephy ActPack 4.1 actuator, providing high torque density, low backlash, and compact packaging suitable for portable prosthetic applications. Control is achieved using an ESR-Adapted Hybrid Kinematic–Impedance Controller (HKIC), which modifies kinematic constraints for incline walking to maintain proper foot–ground alignment and adjusts stance-phase impedance surfaces to compensate for the reduced ankle contribution on declines. Motion capture data from prior literature, comprising ten participants across three speeds and five inclines were used to simulate 150 conditions, enabling estimation of required knee torques and motor demands. Results demonstrate that the proposed architecture and control approach can reproduce biomechanically appropriate knee behavior across slopes, supporting the feasibility of a lightweight, hybrid powered-knee, passive-ankle design.**

## I. Introduction

Lower-limb amputations substantially alter the biomechanics and energetics of walking, inclined locomotion, and other activities of daily living. Passive ankle-foot and knee prostheses, while lightweight and durable, cannot generate net-positive mechanical work, forcing users to compensate through exaggerated hip motions and increased reliance on the sound limb [1], [2]. Furthermore, the inability to replicate normative ankle impedance modulation during stance limits the biomechanical realism of passive devices [3]. These compensations contribute to elevated metabolic energy consumption, musculoskeletal overuse injuries, joint degeneration, and long-term secondary conditions [1], [2]. A central design challenge is therefore the restoration of biomechanically appropriate joint torques and kinematics across a wide range of mobility tasks.

Powered prostheses offer a pathway to restoring more normative mechanics. Early work demonstrated the feasibility of self-contained powered knee–ankle devices capable of producing biomimetic stance-phase knee flexion, positive work during stair ascent, and controlled negative power during descent [4]. Their finite-state impedance control architecture established the canonical framework in which knee and ankle torques are modulated as functions of joint angle, velocity, and state-dependent stiffness and damping [5]. Subsequent work expanded these concepts toward continuous, phase-based representations that reduce hand-tuning and better capture human joint impedance modulation during locomotion [6], [7].

Despite these advances, a recurring insight across the literature is that different joints demand different levels of active control. The knee exhibits substantial positive and negative work during early and mid-stance, especially during tasks with high knee workload, such as incline ascent, requiring high-powered actuation to avoid large compensations [8]. Series-elastic actuator architectures with clutching mechanisms have been proposed to meet these power demands while reducing motor size and electrical load [9]. In contrast, the ankle's torque–angle behavior during level walking and many transitional tasks, is dominated by passive, spring-like mechanics [10]. Modern quasi-passive ankles with variable stiffness or equilibrium shift mechanisms can provide highly functional torque–angle responses with minimal energetic cost and without the thermal or electrical constraints of a powered joint [11], [12]. This motivates a hybrid architecture: a powered knee for tasks involving high mechanical work, paired with a passive or quasi-passive ankle providing compliant energy storage and return.

Recent open-source platforms have further demonstrated the feasibility of high-performance powered knee actuation in portable systems. The Open Source Leg (OSL) integrates brushless DC motors, series elasticity, and optimized belt-drive transmissions to achieve high torque density, low intrinsic impedance, and well-characterized thermal behavior [2]. Its characterization data, including torque bandwidth, thermal time constants, and electromechanical efficiency, provides an ideal engineering foundation for simulation-based analyses of power, current draw, and actuator sizing.

For control, modern phase-based variable impedance controllers have shown strong promise for adapting across speeds, inclines, and stair environments with minimal tuning [6]. Data-driven hybrid kinematic–impedance strategies can produce biomimetic joint trajectories and joint work even in demanding scenarios such as stair ascent and descent [13], [14]. Importantly, several of these controller architectures can be adapted for systems where only the knee is powered, provided the ankle mechanics allow sufficient functional range of motion for the task. Knee-only control has demonstrated strong performance for tasks such as level walking [15], and recent work has explored the adaptations required to knee

*This work was not supported by any organization

[1]Department of Robotics, [2]Department of Mechanical Engineering, University of Michigan, contact: {grinberg, narmph, prioja, seelhoff} @umich.edu

control to allow for inclined walking [16].

Building on this, the present work aims to design, model, and simulate a powered-knee, passive-ankle prosthesis capable of supporting multiple mobility tasks, including level-ground walking and incline locomotion. We combine biomechanical data, actuator/transmission modeling, electrical and thermal simulations, and phase-based control strategies to derive system specifications aligned with human joint demands. This project ultimately seeks to identify design parameters, such as gear ratio, motor constants, thermal limits, and passive ankle stiffness, that enable safe, efficient, and biomimetic assistance across activities central to community ambulation.

## II. Motivation

Transfemoral amputees face substantial challenges in reproducing the biomechanics of healthy locomotion because passive prosthetic knees and ankles cannot generate the joint work or impedance modulation required for natural gait. The absence of active knee power during early stance, flat walking, or demanding tasks such as incline walking forces users to adopt compensatory strategies–such as hip hiking, vaulting, and increased reliance on the sound limb–which elevate metabolic energy expenditure and contribute to long-term musculoskeletal issues [1], [2]. Although powered knee–ankle prostheses can restore much of the missing joint function, fully actuated systems introduce added mass, electrical complexity, and strict thermal constraints that limit practicality for daily community ambulation.

A promising alternative is a hybrid configuration that combines a powered knee with a passive or quasi-passive ankle. This architecture is motivated by the distinct biomechanical roles of the two joints: the knee performs substantial positive and negative work, particularly during tasks, while the ankle behaves predominantly as an elastic energy-storage element during level walking and moderate inclines [10], [11]. Leveraging passive ankle mechanics reduces system complexity and improves energetic efficiency, while concentrating actuation at the knee enables reproduction of the high-power phases of gait most critical for functional mobility. The goal of this project is therefore to identify actuator, transmission, and control parameters that enable a powered-knee, passive-ankle prosthesis to deliver biomechanically appropriate assistance across both level-ground walking and incline locomotion while remaining feasible from electrical and thermal perspectives.

## III. Methods

### A. Mechanical Design

The CycloStride prosthetic knee employs a cycloidal transmission to meet the high torque and precision requirements of level and ramp walking while maintaining a compact, efficient design. Cycloidal drives were selected for their combination of high torque density, low backlash, shock load resistance, durability, and efficiency. High torque density allows the drive to generate the joint torques required to support body weight, particularly during stance and sit-to-stand motions, while low backlash ensures precise control of knee angles, improving gait stability and safety. The geometry of the cycloidal drive also distributes forces across multiple pins, enabling the mechanism to absorb shocks from daily ambulation, while rolling and sliding contact reduces wear under intermittent loads, contributing to a long operational life. Single-stage efficiency of a cycloidal drive is typically between 70–95%, minimizing battery power loss in the powered knee.

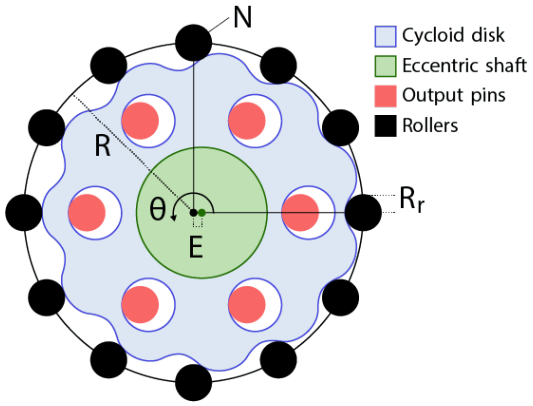


Fig. 1. Cyloidal drive schematic identifying the main components. Cycloid disk (blue), eccentric shaft (green), output pins (red), and rollers (black) and the associated dimensional parameters.

The transmission derives its name from the cycloid curve, traced by a point on a circle rolling along a straight line without slipping. Variations include the epicycloid, formed when rolling on the circumference of another circle, and the epitrochoid, where the tracing point is offset from the rolling circle's center. CycloStride's cycloidal disk profile is based on the epitrochoid, which enables smooth rolling contact and evenly distributed load across multiple points of engagement. The disk geometry is defined by parametric Equations 1, 2, 3 that depend on the disk radius ($R$), rollers radius ($R_r$), shaft eccentricity ($E$), number of rollers ($N$), and rotational angle ($\theta$). A phase shift between the cycloidal disk and the output pins ensures continuous engagement and low backlash, enabling efficient torque transmission. (See Figure 1).

$$X = Rcos(\theta) - R_r cos(\theta - \phi) - Ecos(N\theta) \quad (1)$$

$$Y = -Rsin(\theta) + R_r sin(\theta - \phi) - Esin(N\theta) \quad (2)$$

$$\phi = -\tan^{-1}\left[\frac{\sin(1-N)\theta}{\left(\frac{R}{EN}\right) - \cos((1-N)\theta)}\right] \quad (3)$$

where $0° \leq \theta \leq 360°$.

*1) Transmission Ratio:* The overall transmission ratio $\eta$ is determined by Equation 4,where the number of lobes on the cycloidal disk ($N_L$) and the number of rollers ($N$)

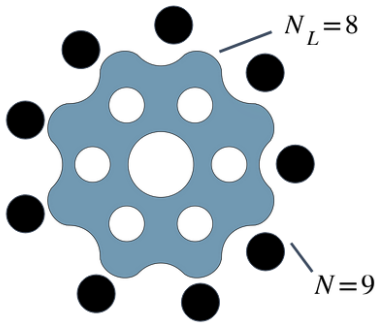


Fig. 2. Designed cycloidal disk showing 8 lobes ($N_L = 8$) and 9 rollers ($N = 9$), resulting in a transmission ratio of 1:8. When combined with the Dephy Act-Pack motor's 1:6 reduction, this yields a total transmission ratio of 1:48 for the system.

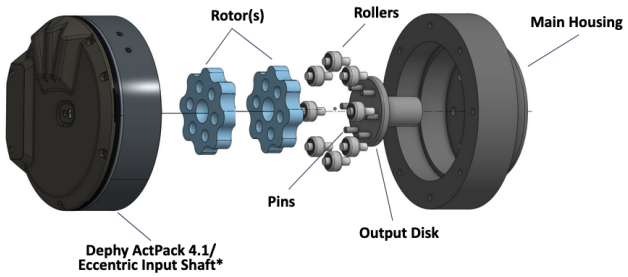


Fig. 3. Exploded view of the CycloStride transmission assembly. The Dephy ActPack motor serves as the input, driving the eccentric shaft. For clarity, the shaft and one roller are omitted. A double cycloidal disk (rotor) assembly reduces vibration. This compact design achieves the target reduction with low backlash and high efficiency for precise prosthetic knee control.

define the ratio, balancing mechanical advantage with torque requirements. (see Figure 2). Based on the Reznick Dataset [17], the knee experiences a maximum peak torque of approximately 0.5 Nm/kg. For an 80 kg user, this corresponds to a peak output torque of roughly 40 Nm. However, based on prior experimentation and to account for unmodeled dynamic loads, a more conservative target of approximately 120 Nm peak torque was selected. Considering an estimated system efficiency of 80%, this design provides a safety factor of around 1.5, ensuring reliable performance during both level and ramp walking.

$$\eta = \frac{N_L}{N - N_L} \tag{4}$$

The cycloidal drive is directly coupled to the Dephy ActPack motor, which provides high-speed brushless actuation with integrated sensors. The motor output drives the eccentric shaft of the cycloidal stage, which rotates the output pins to generate the desired knee torque. The transmission employs a double cycloidal disk (rotor) assembly to reduce vibration and improve load distribution. Radial loads are supported by high-precision needle roller bearings, while any axial forces are accommodated by integrated thrust bearings, ensuring smooth operation and minimal backlash. This integrated configuration achieves the target reduction ratio, maintains high efficiency, and fits within the compact envelope necessary for a portable prosthetic knee. Together, motor and cycloidal transmission enable CycloStride to reproduce normative knee biomechanics while minimizing power consumption and maintaining precise control of joint motion. An exploded view (see Figure 3) of the assembly illustrates the layout of the motor, eccentric shaft, cycloidal disk, and output pins, highlighting the compact and robust design.

### *B. Control Strategy*

To control our powered-knee, passive-ankle prosthesis, we implemented a Hybrid Kinematic Impedance Controller (HKIC), first utilized in [6] to control a powered knee-ankle prosthesis. This control paradigm has seen limited use on powered-knee, passive-ankle devices [15] due to the distinct differences in ankle kinematics on inclines and declines, where ESR feet cannot replicate the necessary ankle range of motion to follow normative ankle behaviors outside of level walking. As such, we must adapt HKIC for use with an ESR foot on both inclines and declines.

*1) Kinematic model and Impedance surface generation:* The methods used to generate the kinematic model, used for swing phase proportional-derivative (PD) position control, and the impedance surfaces, used for stance phase impedance control, are identical to the methods proposed in each method's respective initial manuscript [18], [6]. For brevity, we only discuss the *alterations* proposed by the ESR-Adapted HKIC framework below. The *task space* we are considering for our controller is the same space that the Reznick Dataset [17] utilizes, with walking speeds $\nu \in [0.8, 1.2]$ meters per second and ground slopes $\gamma \in [0, 10]$degrees.

*2) Kinematic and Kinetic modifications for inclined walking:* Previous work has established the need to adapt to ESR feet on inclined walking [16]. While this work directly modified the kinematic optimization objective itself to minimize error to stance-phase foot angle, we instead propose a less restrictive approach to modifying the knee kinematics, with the same intention of restoring favorable ground contact.

First, we assume the prosthetic ankle is perfectly rigid, i.e. $\theta_{ankle} = 0$. Then, we define the foot angle $\theta_{foot}$ relative to the other lower-body joint angles in the following equation:

$$\theta_{foot} = \theta_{hip} - \theta_{pelvis} - \theta_{knee} \tag{5}$$

because the ankle is assumed to be rigidly fixed in its neutral position, i.e. $\theta_{ankle} = 0$. To ensure the foot lands on the prosthetic heel rather than the keel, we desire to impose the same *relative* difference in angle between the foot and the ground slope at heel strike:

$$\theta_{foot} - \theta_{ground} \geq \theta_{foot,AB} - \theta_{ground} \Rightarrow \theta_{foot} \geq \theta_{foot,AB} \tag{6}$$

where $\theta_{foot}$ denotes prosthetic foot angle, $\theta_{foot,AB}$ denotes normative foot angle, and $\theta_{ground}$ denotes ground slope. Combining this equation with Equation 5 yields on optimization constraint at Heel Strike:

$$\theta_{knee} \leq \theta_{hip} - \theta_{pelvis} - \theta_{foot,AB} \tag{7}$$

The introduced constraint results in altered kinematics throughout stance phase, necessarily requiring different impedance surfaces to render normative torques. We did not modify the impedance surface optimization for inclined walking tasks, and thus the framework outlined in [6] describes our methodology.

*3) Kinetic modifications for declined walking:* For declined walking, ankle range of motion is quite similar to that of level walking, and as such, no kinematic modifications are needed. However, the kinetics required of the powered knee prosthesis will differ from able-bodied kinetics, as the ESR foot can no longer provide a braking impulse during stance phase, which is crucial for regulating body motion and overall speed for declined walking [19] It becomes clear that we will need to prioritize the impedance model to provide damping torque rather than spring torque throughout stance phase. In order to accomplish this, we implement a penalty term similar to that implemented in Equations 15-19 of [13] which penalizes only torque generated by the spring terms, allowing more torque to be provided by damping and generating a more passive gait instead of unnecessarily injecting more energy into the user.

### C. Control Simulation

*1) Software Overview:* All simulation was performed in MATLAB version R2025a (MathWorks, Natick, MA.) In order to evaluate required torques from the knee prosthesis motor, we simulated the device by replicating the motion capture data collected from [17] for all $n = 10$ participants across each recorded steady-state task (3 walking speeds and 5 inclines), yielding 150 simulated tasks in all. To generate kinematic and impedance control surfaces, the specific-task results are linearly interpolated with respect to both walking speed and incline to generate continuous surfaces.

For each task, the prosthesis was commanded to follow the knee kinematics, modified as necessary for inclined walking as discussed in Section III-B.2. We assumed perfectly linear phase and assumed that toe-off occurred consistently at 64 percent the way through the gait cycle [17]. In stance phase, the impedance controller was called to generate the torque depending on the current knee position and velocity. In swing phase, the position controller was called in a similar fashion. The two controllers can have their control laws combined to represent a general control law:

$$\tau_{knee} = InSwing \cdot \tau_{PD} + InStance \cdot \tau_{Impedance} \tag{8}$$

where $InSwing$ and $InStance$ are boolean expressions evaluating whether the controller is in swing or stance phase.

Knowing our transmission ratio from the joint to the motor, we can calculate the necessary motor torque and velocity as follows:

$$\tau_{motor} = \frac{\tau_{knee}}{(N1 \cdot N2 \cdot \eta)}; \dot{\theta}_{motor} = N1 \cdot N2 \cdot \dot{\theta}_{knee} \tag{9}$$

where $N1 = 6$ and $N2 = 8$ are our ActPack and Cycloidal reduction ratios, and our overall transmission efficiency $\eta$ is assumed to be 80%.

We then can rearrange Kirchhoff's Voltage Law and Newton's Second Law to determine our required current and voltage, numerically differentiating the motor velocity as needed:

$$v_w(t) = i_w(t)R + L\frac{d}{dt}i_w(t) + k_t\dot{\theta}_{motor}(t) \tag{10}$$

$$i_w(t) = \frac{1}{k_t}(J_m\ddot{\theta}_{motor}(t) + b_m\dot{\theta}_{motor}(t) + \tau_{motor}(t)) \tag{11}$$

with motor phase resistance $R_\phi = 0.315\Omega$, inductance $L = 138\mu H$, motor constant $k_t = 0.12\frac{Nm}{A}$ and damping constant $b_m = 0.16\frac{mNm \cdot s}{rad}$ [20].

### D. Motor Selection

We selected the Dephy ActPack 4.1 in the 1:6 gearing configuration as the actuator for the CycloStride. This actuator is already used in powered knee prostheses [2], and its electromechanical properties have been thoroughly characterized in prior literature [20], [21]. By reconfiguring Equations 10 and 11, we calculated the no-load speed, $\dot{\theta}_{\text{no load}}$, and stall torque, $\tau_{\text{stall}}$, using the maximum voltage and current specifications provided in [20]. The calculated $\dot{\theta}_{\text{no load}}$ and $\tau_{\text{stall}}$ are 299.1 rad/s and 3.44 Nm, respectively.

Referring to the torque-speed relationship driven by the HKIC controller (Figure 6), this actuator is well-specced for the required torque demands; however, it is slightly underspecced regarding peak velocity. This speed saturation is most likely to occur during the swing phase of walking, which may necessitate minor compensatory gait deviations from the user.

### E. Thermal Modeling and Simulation

To ensure the motor operates within safe thermal limits during extended use, we modeled the thermal losses of the system. We characterized the heating of the motor winding and the housing separately using two transfer functions, where each model describes the relationship between heat flux and the temperature change of the respective component. Summing these transfer functions allows us to model the thermal dynamics of the actuator as a whole.

By defining a thermal time constant, $\tau$, as the product of thermal resistance, $R$, and thermal capacitance, $C$, we simplify the model as shown in Equation 13. Here, the heat flux of the motor is represented as $Q(s)$ and the temperature rise across the motor as $\sigma(s)$.

$$\frac{\sigma(s)}{Q(s)} = \underbrace{\frac{R^{ha}}{R^{ha}C^h s + 1}}_{\substack{\text{Temp rise across housing} \\ \text{from heat flux}}} + \underbrace{\frac{R^{wh}}{R^{wh}C^w s + 1}}_{\substack{\text{Temp rise across winding} \\ \text{from heat flux}}} \tag{12}$$

$$= \frac{R^{ha}}{\tau^h s + 1} + \frac{R^{wh}}{\tau^w s + 1} \tag{13}$$

The thermal resistances for the housing/atmosphere ($R^{ha}$) and winding/housing ($R^{wh}$), as well as the housing and

winding time constants ($\tau^h$ and $\tau^w$), were previously estimated in [20]. These properties (Table I) were derived by minimizing the sum-squared error between the measured temperature rise of the actuator and the estimated rise predicted by Newton's law of cooling.

| Parameter | Value |
|---|---|
| $R^{wh}$ (K/W) | 1.1 |
| $R^{ha}$ (K/W) | 3.5 |
| $\tau^h$ (s) | 670.6 |
| $\tau^w$ (s) | 65.0 |

TABLE I

THERMAL PROPERTIES ESTIMATED IN [20]

We estimate the heat flux of the actuator during level and inclined walking using Equation 14, where $i_w$ is the current commanded by the control framework and $R$ is the terminal resistance of the actuator.

$$Q = i_w^2 R \tag{14}$$

To simulate the thermal load of continuous ambulation, we replicated the strides from the Reznick dataset repeatedly. Using the model in Equation 13, the parameters in Table I, and the flux estimation from Equation 14, we estimated the temperature rise of the actuator across all target slopes and walking speeds.

## IV. RESULTS

### A. Control Surfaces

Figure 4 shows the resulting kinematic surfaces for all tasks combined into one plot. The underlying surface represents the interpolated task space for a fixed speed of 1 meter per second, showing the varied changes to otherwise-normative kinematics. While the stance-phase trajectories in this plot (Percent Gait $<$ 64%) are not directly used as references for control, they are the driving force behind the equilibrium angle surfaces for stance-phase impedance control. The trajectories for positive-slope ramps show distinctly different trajectories compared to normative data [17], showing the need for modifying reference knee kinematics for use with ESR feet.

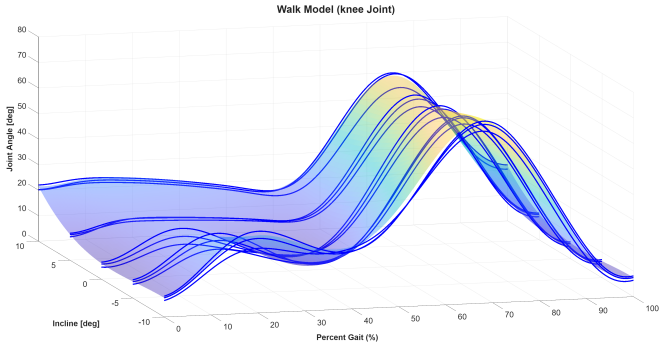


Fig. 4. Knee Kinematic surface for all walking tasks (blue lines.)

Figure 5 shows, from left to right, the stiffness, damping, and equilibrium angle surfaces utilized in stance-phase impedance control. General patterns emerge: stiffness is highest at heel strike across all tasks, slowly dropping towards the end of stance phase. Damping is relatively low across the board except for declined walking, where we specifically prioritized an increase in damping torque to make the knee render more passive mechanics during ramp descent. Equilibrium angle is near-monotonically increasing throughout stance phase, with greater increases happening during push-off to help the prosthesis unload for swing phase. The resulting torque output from this model, when following the kinematic trajectories shown in Figure 4, was compared to normative able-bodied torques from [17], with normalized Root Mean Squared Error (RMSE) reported in Table II. It is worth noting that more extreme slopes have the worst RMSE, as these are where the generated kinematics (and thus kinetics) are most different from normative walking. Unsurprisingly, the unaffected level-ground condition shows the lowest RMSE of around 0.12 Nm/kg across all three walking speeds.

| TASKS | 0.8 m/s | 1.0 m/s | 1.2 m/s |
|---|---|---|---|
| -10 deg | 0.2500 | 0.2799 | 0.3028 |
| -5 deg | 0.1731 | 0.1906 | 0.2246 |
| 0 deg | 0.1374 | 0.1227 | 0.1374 |
| +5 deg | 0.1970 | 0.1946 | 0.1966 |
| +10 deg | 0.2350 | 0.2245 | 0.2208 |

TABLE II

NORMALIZED ROOT MEAN SQUARED ERROR (RMSE) OF STANCE-PHASE TORQUE

### B. Thermal Simulation

The Dephy ActPack 4.1 has a safety shut-off temperature of 70°C [21]. Assuming an ambient temperature of 25°C, the thermal modeling results (Figure 8) indicate that for all speeds and slopes, except for the 10-degree incline condition, steady-state temperatures remain well below this safety threshold. In the 10-degree incline cases, the model predicts that the actuator reaches the safety shut-off temperature only after approximately ten minutes of continuous operation. This exceeds the typical time a user would spend on such a steep incline during daily ambulation. Consequently, the slopes encountered during everyday activities and even easy-to-moderate hiking fall within the safe operating range of the CycloStride.

## V. LIMITATIONS AND FUTURE WORK

The integration of a cycloidal transmission in a powered prosthetic knee involves several design considerations that influence performance and reliability. The drive relies on tight tolerances in the rollers and their placement to ensure uniform load sharing. Small errors in roller diameter, spacing, or alignment, as well as wear over time, can disrupt this balance and lead to increased vibration and localized stress concentrations. The cycloidal disk profile must also be manufactured accurately, as deviations from the intended geometry can degrade rolling contact and increase contact

forces. In addition, eccentricity and bearing alignment between the motor shaft and cycloidal stage must be carefully controlled; misalignment can introduce additional friction, uneven loading, and premature bearing wear. Transmission losses increase during low-speed, high-torque operation typical of stance phase due to rolling–sliding contact and bearing friction, which may reduce efficiency relative to idealized estimates. The high transmission ratio and rolling contact inherent to the cycloidal mechanism also result in relatively low backdrivability, which may limit passive knee motion and increase apparent joint impedance when the actuator is unpowered or during low-torque phases of gait. This behavior places greater reliance on active control strategies to ensure smooth swing dynamics and user comfort. Finally, compact integration of the cycloidal drive constrains bearing size and lubrication volume, which may limit long-term durability under continuous daily loading without careful material selection and maintenance strategies.

While Hybrid Kinematic Impedance Control has been validated across several prosthetic devices and studies [6], [7], there is still limited data on how this control paradigm could be adapted for powered-knee, passive-ankle devices. The only studies with HKIC on this kind of system could transfer only between level walking and sitting/standing activities [15]. Future work would involve a more robust controller with high level activity recognition and classification, as has been done on the multi-joint implementation of the controller across stairs and other activities [14], [22]

The Dephy ActPack is slightly under-specified regarding maximum velocity. The calculated no-load speed of roughly 300 rad/s approaches the kinematic limits of the knee during the swing phase of gait at higher walking speeds and declines. This saturation may prevent the controller from achieving peak velocity, potentially resulting in a stiff swing phase or forcing the user to adopt compensatory gait patterns to ensure toe clearance. Future iterations of control parameters and surfaces could take this limitation into account, giving a slightly slower knee velocity in swing phase which may lead to worse tracking of normative kinematics.

The thermal performance presented here is based on simulation using parameters characterized in prior literature. These models assume constant convective cooling conditions and do not account for environmental variations such as variable ambient temperatures and terrains. Long-term benchtop testing and clinical trials are required to validate these thermal predictions and ensure the device remains safe during extended use in diverse environments.

## REFERENCES


[1] S. K. Au, J. Weber, and H. Herr, "Powered ankle-foot prosthesis improves walking metabolic economy," *IEEE Transactions on Robotics*, vol. 25, no. 1, pp. 51–66, 2009.

[2] A. F. Azocar, L. M. Mooney, J.-F. Duval, A. M. Simon, L. J. Hargrove, and E. J. Rouse, "Design and clinical implementation of an open-source bionic leg," *Nature Biomedical Engineering*, vol. 4, pp. 941–953, 2020.

[3] E. J. Rouse, L. J. Hargrove, E. J. Perreault, and T. A. Kuiken, "Estimation of human ankle impedance during the stance phase of walking," *IEEE Transactions on Neural Systems and Rehabilitation Engineering*, vol. 22, no. 4, pp. 870–878, 2014.

[4] F. Sup, H. A. Varol, J. Mitchell, T. J. Withrow, and M. Goldfarb, "Self-contained powered knee and ankle prosthesis: Initial evaluation on a transfemoral amputee," in *IEEE International Conference on Rehabilitation Robotics (ICORR)*, 2009, pp. 638–644.

[5] H. A. Varol, F. Sup, and M. Goldfarb, "Multiclass real-time intent recognition of a powered lower limb prosthesis," *IEEE Transactions on Biomedical Engineering*, vol. 57, no. 3, pp. 542–551, 2010.

[6] T. K. Best, C. G. Welker, E. J. Rouse, and R. D. Gregg, "Data-driven variable impedance control of a powered knee-ankle prosthesis for adaptive speed and incline walking," *IEEE Transactions on Robotics*, vol. 39, no. 3, pp. 2151–2169, 2023.

[7] T. K. Best, G. C. Thomas, S. R. Ayyappan, R. D. Gregg, and E. J. Rouse, "A compensated open-loop impedance controller evaluated on the second-generation open-source leg prosthesis," *IEEE/ASME Transactions on Mechatronics*, pp. 1–13, 2024.

[8] T. Elery, S. Rezazadeh, C. Nesler, and R. D. Gregg, "Design and validation of a powered knee-ankle prosthesis with high-torque, low-impedance actuators," *IEEE Transactions on Robotics*, vol. 36, no. 6, pp. 1649–1668, 2020.

[9] E. J. Rouse, L. M. Mooney, and H. M. Herr, "Clutchable series-elastic actuator: Implications for prosthetic knee design," *The International Journal of Robotics Research*, vol. 33, no. 13, pp. 1611–1625, 2014.

[10] M. K. Shepherd and E. J. Rouse, "The VSPA foot: A quasi-passive ankle-foot prosthesis with continuously variable stiffness," *IEEE Transactions on Neural Systems and Rehabilitation Engineering*, vol. 25, no. 12, pp. 2375–2386, 2017.

[11] J. D. Lee, L. M. Mooney, and E. J. Rouse, "Design and characterization of a quasi-passive pneumatic foot-ankle prosthesis," *IEEE Transactions on Neural Systems and Rehabilitation Engineering*, vol. 25, no. 7, pp. 823–831, 2017.

[12] M. K. Shepherd and E. J. Rouse, "Design of a quasi-passive ankle-foot prosthesis with biomimetic, variable stiffness," in *IEEE International Conference on Robotics and Automation (ICRA)*, 2017, pp. 6672–6678.

[13] R. J. Cortino, T. K. Best, and R. D. Gregg, "Data-driven phase-based control of a powered knee-ankle prosthesis for variable-incline stair ascent and descent," *IEEE Transactions on Medical Robotics and Bionics*, vol. 5, no. 4, pp. 175–188, 2023.

[14] S. Cheng, C. A. Laubscher, and R. D. Gregg, "Controlling powered prosthesis kinematics over continuous inter-leg transitions between walking and stair ascent/descent," *IEEE Transactions on Neural Systems and Rehabilitation Engineering*, vol. 32, pp. 3819–3830, 2024.

[15] T. K. Best, C. A. Seelhoff, J. Wensman, and R. D. Gregg, "The clinical effects of the Össur power knee with phase-based and default control during sitting, standing, and walking," *Journal of NeuroEngineering and Rehabilitation*, vol. 22, no. 200, 2025.

[16] C. A. Seelhoff, T. K. Best, and R. D. Gregg, "Adapting biomimetic kinematics for controlling a powered-knee, passive-ankle prosthesis across inclines," in *IEEE International Conference on Rehabilitation Robotics (ICORR)*, 2025.

[17] E. Reznick, K. R. Embry, R. Neuman, E. Bolívar-Nieto, N. P. Fey, and R. D. Gregg, "Lower-limb kinematics and kinetics during continuously varying human locomotion," *Scientific Data*, vol. 8, no. 1, p. 282, Oct. 2021, number: 1 Publisher: Nature Publishing Group. [Online]. Available: https://www.nature.com/articles/s41597-021-01057-9

[18] T. K. Best, K. R. Embry, E. J. Rouse, and R. D. Gregg, "Phase-Variable Control of a Powered Knee-Ankle Prosthesis over Continuously Varying Speeds and Inclines," in *2021 IEEE/RSJ Int. Conf. Intell. Robot. and Syst. (IROS)*, Sep. 2021, pp. 6182–6189, iSSN: 2153-0866.

[19] J. S. Gottschall and R. Kram, "Mechanical energy fluctuations during hill walking: the effects of slope on inverted pendulum exchange," *Journal of Experimental Biology*, vol. 209, no. 24, pp. 4895–4900, Dec. 2006. [Online]. Available: https://doi.org/10.1242/jeb.02584

[20] U. H. Lee, C.-W. Pan, and E. J. Rouse, "Empirical characterization of a high-performance exterior-rotor type brushless DC motor and drive," in *IEEE/RSJ International Conference on Intelligent Robots and Systems (IROS)*, 2019.

[21] *ActPack 4.1*, Dephy, 2023. [Online]. Available: https://drive.google.com/file/d/1k99Pfd8xSigBUOtTD9PhqQm5TaQjvgVz/view

[22] A. E. Lang, C. A. Laubscher, S. Cheng, and R. D. Gregg, "Vibrotactile haptic and gesture feedback in a smartwatch for controlling a multi-activity powered knee-ankle prosthesis," in *2025 47th Annual International Conference of the IEEE Engineering in Medicine and Biology Society (EMBC)*, 2025, pp. 1–5.

# APPENDIX

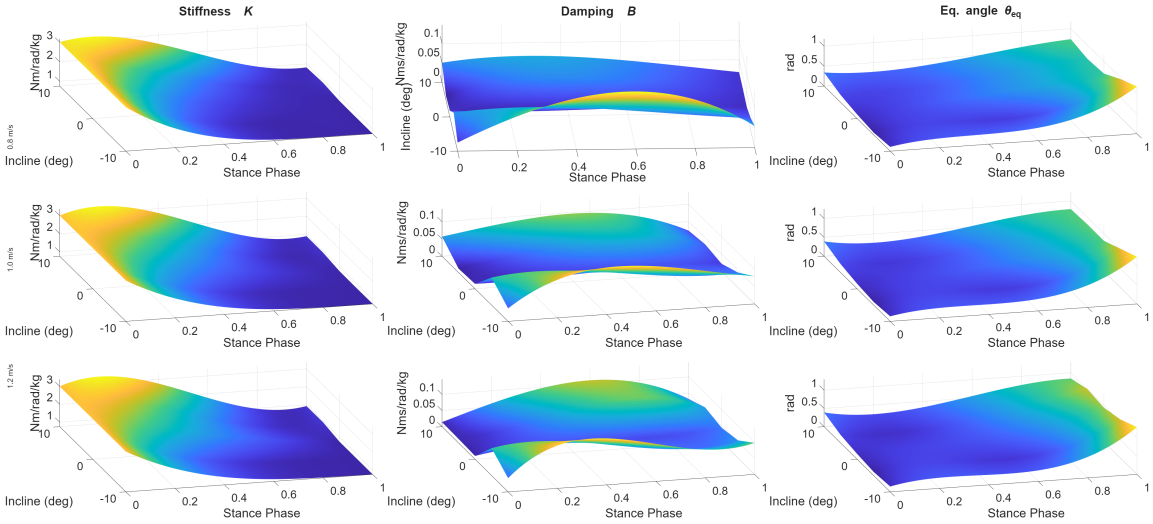


Fig. 5. Impedance Surfaces for all walking tasks.

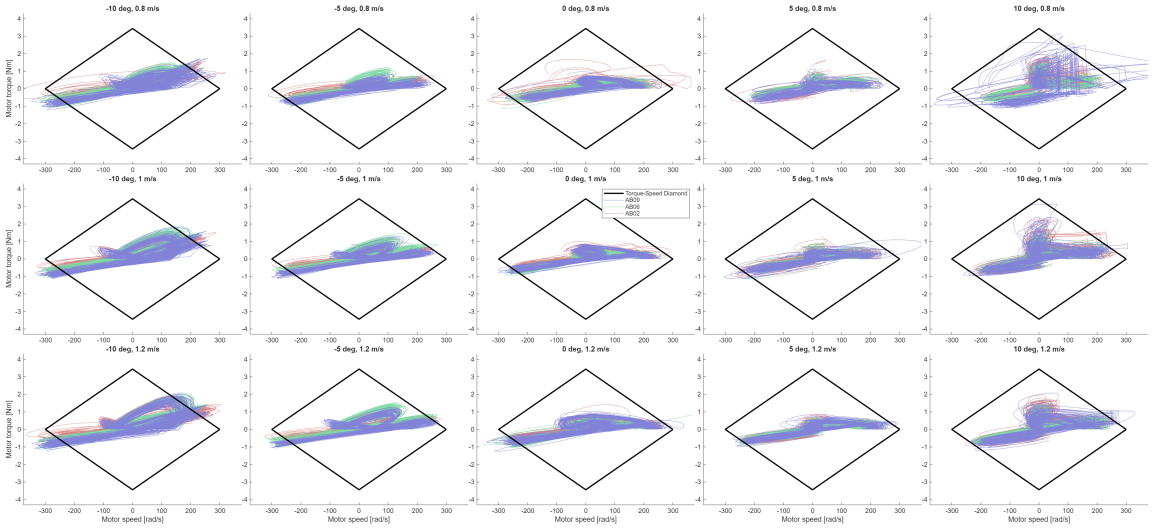


Fig. 6. Torque-Speed Diamonds for selected subjects across all walking tasks.

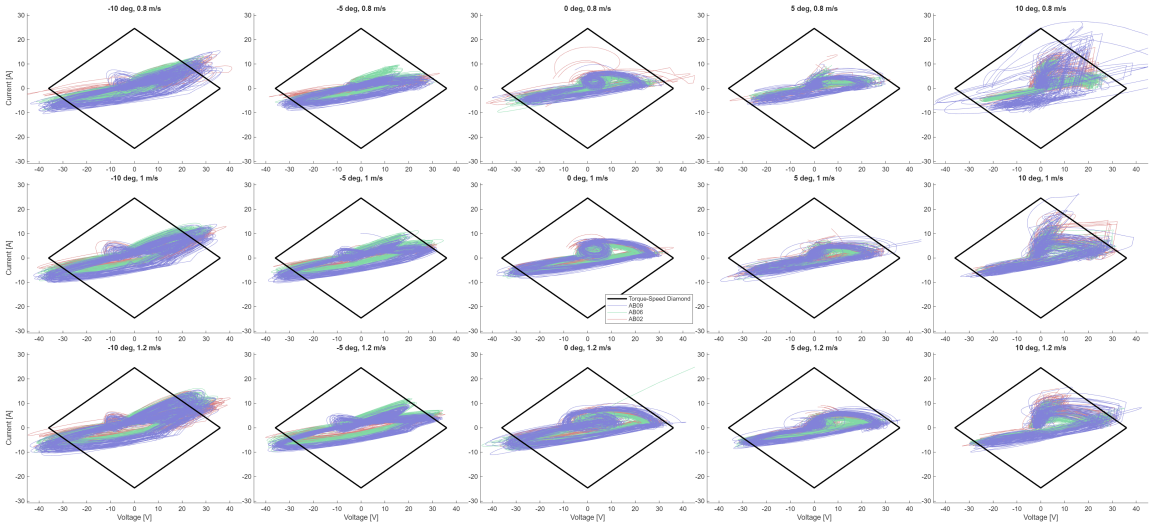


Fig. 7. Current-Voltage Diamonds for selected subjects across all walking tasks.

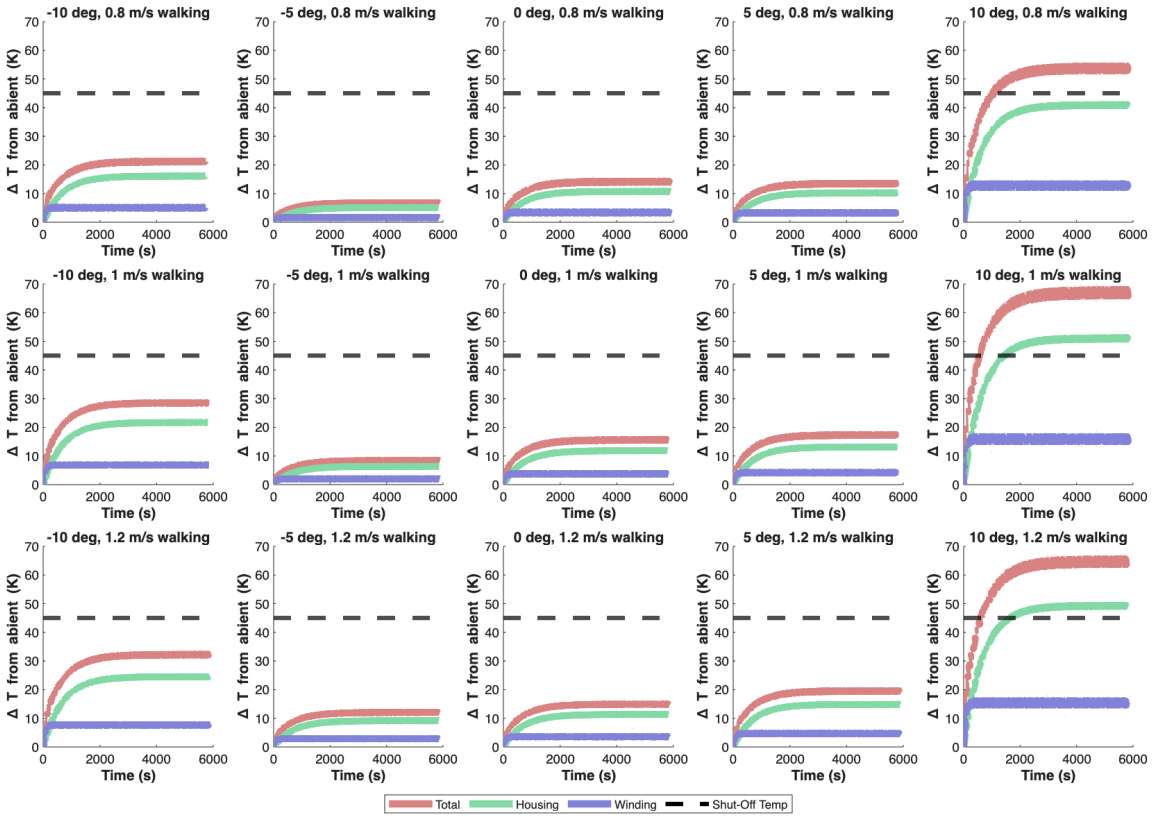


Fig. 8. Temperature rise over 5000 strides for every walking speed and slope of interest.